E. Adrover*, D. Boldrini, N.J. Divins, A. Casanovas, G. Tonetto, E. López and J. Llorca*

Study of Cu-Zn and Au/TiO_2 Catalysts on Anodized Aluminum Monoliths for Hydrogen Generation and Purification

DOI 10.1515/ijcre-2015-0119

Abstract: This work reports the preparation of Cu-Zn and Au/TiO_2 catalysts on anodized aluminum monoliths (AAM). The structured catalysts were studied for the generation of H_2 by methanol steam reforming (MSR) and its purification by preferential oxidation of CO (CO-PrOx). Initially, it was possible to generate a surface with whiskers and larger surface area by hydrothermal treatment of the AAM. Subsequently, the structured catalysts were synthesized by incipient wetness impregnation (IWI) and hydrothermal synthesis (HS). IWI synthesis allowed for the deposition of a larger amount of catalytic material than HS, with very good adhesion. The TiO_2-IWI structured catalyst presented a homogeneous catalytic coating, with the presence of agglomerated particles. On the other hand, Cu-Zn-IWI showed good dispersion of the deposited particles with a homogeneous surface coating. EDX analysis corroborated the presence of Ti, Cu and Zn in all the catalytic surfaces. The incorporation of Au over TiO_2-IWI structured catalysts was successfully performed by IWI using a colloidal solution of gold nanoparticles. MSR was studied over the developed metallic monoliths functionalized with Cu-Zn by the IWI method. The samples showed promising results in terms of activity, selectivity, and stability. Both diluted and concentrated methanol + water feeds were assayed. Complete methanol conversion was achieved for the diluted feed. Maximum methanol conversions of 55 % with 60 % H_2 yield were measured when the concentrated feed was selected. Promising results were also achieved for the Au-based structured catalysts in the CO-PrOx in an H_2-rich atmosphere. Although CO conversions of approximately 60 % were achieved, operating with higher catalyst loadings would be recommended to reach the high CO conversions required for PrOx catalysts.

Keywords: structured catalysts, anodized aluminum, gold, copper, zinc

***Corresponding authors: E. Adrover,** Planta Piloto de Ingeniería Química (CONICET–UNS), Bahía Blanca, Argentina, E-mail: eadrover@plapiqui.edu.ar
J. Llorca, Institut de Tècniques Energètiques, Universitat Politècnica de Catalunya, Barcelona, Spain, E-mail: jordi.llorca@upc.edu
D. Boldrini, Planta Piloto de Ingeniería Química (CONICET–UNS), Bahía Blanca, Argentina
N.J. Divins, A. Casanovas, Institut de Tècniques Energètiques, Universitat Politècnica de Catalunya, Barcelona, Spain
G. Tonetto, E. López, Planta Piloto de Ingeniería Química (CONICET–UNS), Bahía Blanca, Argentina

1 Introduction

Structured catalysts have gained great importance because they present less pressure drop and mass transfer resistance than conventional heterogeneous catalysts. Anodized aluminum is an interesting alternative as a monolithic substrate, both from the perspective of the metal (price, weight, machinability and thermal conductivity) and of the alumina coating (Sanz et al. 2008). The melting temperature of Al (933 K) limits the use of these monoliths to processes with low to moderate temperatures. The alumina layer generated by anodizing offers interesting prospects, since it is an excellent catalyst support with good adherence and stability. In addition, its texture can be modified by altering the parameters in the anodizing process.

A general interest has emerged recently about the rational and/or decentralized use of energy. In this context, the production and purification of hydrogen for use in fuel cell applications appears as a technologically interesting alternative. Among the different processes proposed, the generation of H_2 by methanol reforming (MSR) and its purification by preferential oxidation of CO (CO-PrOx) are identified as highly suitable for small/medium-scale systems given their simplicity. The use of structured catalysts in these applications has important advantages for the design of the corresponding reactor based on the modular nature of the catalysts and their good ability to manage the associated thermal effects (especially in metal structures) (Cybulski and Moulijn 1998).

Different catalysts have been proposed and tested in the literature for the hydrogen generation (MSR) and purification (CO-PrOx) reactions.

The most common catalysts for MSR are the copper-based ones. However, in order to improve their catalytic activity, the addition of promoters (e. g., Zr, Zn and Mn) and the preparation method have been under study (Sá et al. 2010). MSR has been studied over Cu-Zn based catalysts at temperatures lower than 573 K (Agrell, Birgersson, and Boutonnet 2002; Bichon et al. 2007; Purnama et al. 2004; Sá et al. 2010; Turco et al. 2007; Wu et al. 2009). Zn improved the metal dispersion and reducibility of Cu^{2+} species, generating a positive effect on catalytic activity. There are numerous studies on MSR catalyzed by powder Cu-Zn based catalysts, but less over structured catalysts. Lindström and Pettersson (2002) studied the reaction of methanol steam reforming over various alumina-supported copper-based monolithic catalysts. The cordierite ($2MgO{\cdot}5SiO_2{\cdot}2Al_2O_3$) monolith substrate was initially coated with aluminium oxide (γ-Al_2O_3) to increase the surface area and to enable dispersion of the catalytic material. Recently, Reddy, Lee, and Kim (2015) studied MSR over structured catalysts prepared by electroless deposition of Cu and Zn on anodically oxidized alumina. In their work, the catalysts were pieces with a size of 2–3 mm^2, and they were loaded into a tubular reactor.

In recent years, supported gold nanoparticles have shown remarkable catalytic properties for selective CO oxidation, provided the size of the nanoparticles amounts only few nanometers. In addition to the size of the gold particles, the catalytic activity of supported gold catalysts is recognized to be dependent on the support (Lakshmanan, Park, and Park 2014). Since TiO_2 is almost inert as a catalyst for CO oxidation as is bulk gold, the Au-TiO_2 system can be regarded as the most clear-cut example for investigating the significant synergistic effect between gold and the metal oxide support (Tsubota, Cunningham, and Bando Haruta 1993). Many studies have demonstrated the remarkable catalytic properties of gold nanoparticles supported on TiO_2 particles for selective CO oxidation in H_2-rich streams (Bamwenda et al. 1997; Daté and Haruta 2001; Galletti et al. 2007; Kipnis 2014; Schumacher et al. 2004). However, only few works of CO preferential oxidation over gold based structured catalysts can be found in literature. Lopez, Kolios, and Eigenberger (2005, 2007) proposed a structured folded-plate reactor for CO-PrOx using a Au-based catalyst. Divins et al. (2011) reported CO-PrOx over Au/TiO_2 catalysts. In their work, two different monolithic substrates were studied, namely a silicon micromonolith with 3 μm channel diameter and a conventional cordierite monolith with 400cpsi. Both substrates were functionalized by anchoring carbosilanethiol dendron-protected pre-formed Au nanoparticles over TiO_2. To the best of our knowledge, studies regarding metallic monoliths washcoated with Au/TiO_2 catalysts applied to CO preferential oxidation (in a H_2 rich atmosphere) have not been reported.

This work discusses on the preparation, characterization and reaction tests of structured catalysts profited towards the generation and purification of hydrogen. The catalysts were prepared by incipient wetness impregnation and hydrothermal synthesis on anodized aluminum monoliths (previously modified by hydrothermal treatment). The selected active phases were (a) Cu-Zn for the methanol reforming reaction and (b) Au nanoparticles on TiO_2 for the CO-PrOx reaction. The monolithic systems were tested in the reactions of interest, analyzing their activity, selectivity and stability under different operating conditions.

2 Materials and methods

2.1 Preparation of the anodized aluminum monoliths

The anodized aluminum monoliths were prepared using commercial laminated pure aluminum as metallic substrate. The aluminum sheets were cut in pieces of 15 mm × 18 mm and 15 mm × 23.5 mm. The bigger piece was rolled using a mechanical device made of two Nylon cogwheels.

The operating conditions for the anodizing process were:

- Electrolyte: oxalic acid, $H_2C_2O_4$
- Electrolyte concentration: 1.6 M
- Temperature: 313 K
- Flow density: 1.2 A/dm^3
- Time: 40 min anodizing + 40 min pore opening

After anodizing, the metal sheets were washed and dried (333 K for 30 min). The Al_2O_3/Al monoliths were prepared by rolling around a spindle alternate previously anodized flat and corrugated foils. The final monolith was a cylinder of 14 mm diameter by 15 mm height and a cell density of 350 cells per square inch (cpsi). The monoliths were exposed to the following hydrothermal treatment:

1. Calcination at 773 K for 2 h.
2. Immersion in deionized water at 373 K for 1 h.
3. Drying at 333 K for 1 h, followed by 30 min at 423 K.
4. Calcination at 773 K for 16 h.

2.2 Incorporation of the active phase

The incorporation of TiO_2 and Cu-Zn over the anodized aluminum monoliths was performed by incipient wetness impregnation (IWI) and hydrothermal synthesis (HS).

In the case of TiO_2, for IWI the substrate was impregnated with pure titanium isopropoxide (745 µL). For HS, the substrate and the precursor solution (600 µL of titanium isopropoxide diluted in 50 ml of ethanol) were poured into an autoclave for 4 h at 393 K. These samples were dried under continuous rotation for 1 h at 353 K and calcined at 723 K for 4 h.

Gold was added to the TiO_2/monolith by IWI using a colloidal solution of gold nanoparticles in toluene (Divins et al. 2011).

In the case of Cu-Zn, the target metal loadings were 10 %wt ZnO and 10 %wt CuO (with respect to monolith weight). For IWI, the substrate was impregnated with a solution of copper nitrate trihydrate (0.114 g) and zinc nitrate hexahydrate (0.137 g) dissolved in 600 µL of ethanol. For HS, the same salts (0.548 g $Zn(NO_3)_2.6H_2O$ and 0.456 g $Zn(NO_3)_2.3H_2O$) were dissolved in 50 mL of ethanol and then the mixtures were poured, with the substrate, into an autoclave. The synthesis was performed at 393 K for 4 h. The resulting monoliths were finally dried under continuous rotation for 1 h at 353 K and then calcined at 673 K for 4 h.

The monoliths were named considering the active phase and the synthesis method, for example Cu-Zn deposited by HS on anodized aluminum monolith was named Cu-Zn-HS.

2.3 Characterization

Textural properties were studied by N_2 adsorption-desorption isotherms at 77 K in a Micromeritis ASAP 2020 apparatus with a home-made cell that allows for a complete monolith analysis. Before analysis, the monoliths were degassed for 2 h at 423 K under vacuum.

The morphology and composition of the monolith surface were studied by scanning electron microscopy (SEM) and energy dispersive X-ray analysis (EDX). Secondary electron images were recorded at 20 kV using a JEOL JSM 6400 instrument. High resolution transmission electron microscopy (HRTEM) was carried out with a JEOL JEM 2010F microscope operating with a field emission source at an accelerating voltage of 300 kV.

The amount of alumina generated during anodizing was determined by means of gravimetry. It was calculated from the weight difference of the anodized sheet before and after the chemical treatment which selectively dissolved the alumina layer. The dissolution process was carried out at 538 K for 20 min using a 0.5 M phosphoric acid and 0.2 M chromic acid solution.

The catalyst adhesion on the substrate was estimated by evaluating the weight loss of a catalyst-coated sample treated in an ultrasonic bath (Bandelin SONOREX 10P) at maximum frequency for 30 min.

The XPS measurements were conducted using a multi-technique system (SPECS) equipped with a dual Mg/Al X-ray source and a hemispherical PHOIBOS 150 analyzer operating in the fixed analyzer transmission (FAT) mode. The spectra were obtained with pass energy of 30 eV, and the Mg Kα X-ray source was operated at 100 W. The working pressure in the analyzing chamber was less than 2×10^{-8} mbar. Before measurements, fresh samples were reduced with 10 % H_2 in N_2 at 300 °C for 2 h and transferred without exposure to air.

2.4 Catalytic tests

The reaction performance evaluation of the prepared monoliths was accomplished in a lab-scale kinetic set up, as shown in Schemes 1–3. The catalytic samples were implemented into a tubular stainless-steel reactor disposed in an electric furnace (Heraeus) governed with a PID electronic controller (Novus 480D). A K-type

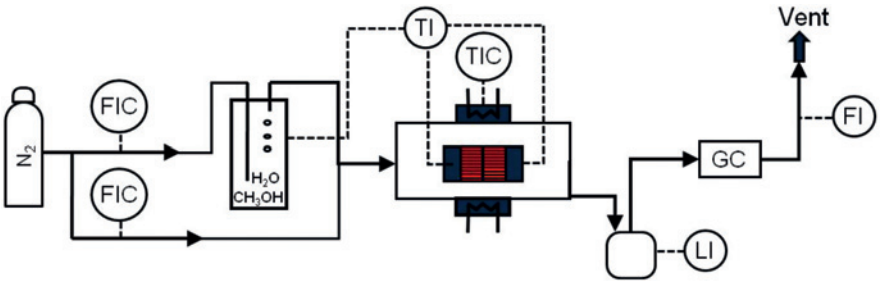

Scheme 1: Experimental setup for methanol reforming with diluted feed.

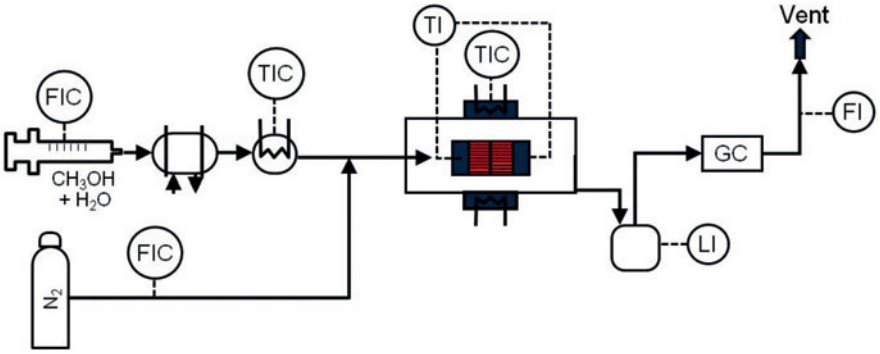

Scheme 2: Experimental setup for methanol reforming with concentrated feed.

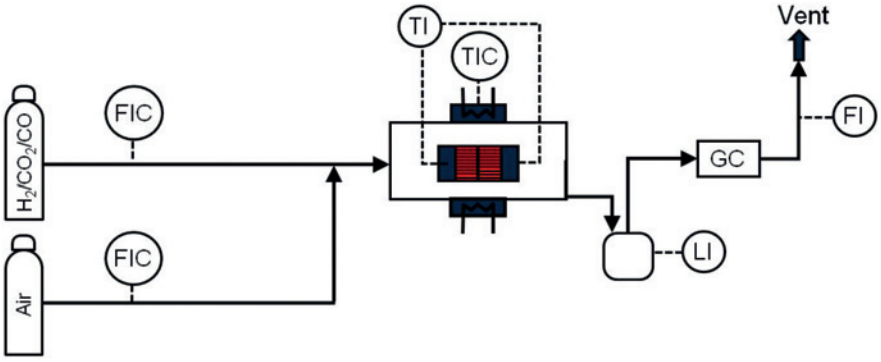

Scheme 3: Experimental setup for CO-PrOx reaction.

thermocouple was additionally used to register the reactor temperature. Schemes 1 and 2 represent the experimental setup employed for methanol steam reforming, while Scheme 3 represents the experimental setup employed for studying the CO-PrOx reaction.

Specifically, Scheme 1 shows the experimental setup for methanol reforming with diluted feed. A nitrogen stream is bubbled through a methanol-water liquid mixture to load saturate amounts of these reactants, which were then fed to the reactor as a diluted feed. A step further, Scheme 2 describes a situation where a realistic feed is dosed to the monolith. Moreover, a liquid mixture of methanol and water is fed by means of a Cole Parmer 74900 syringe pump directly from a storage tank. The subsequent vaporization and overheating of this mixture was performed by using heating tapes. Finally, Scheme 3 displays the experimental setup for CO-PrOx reaction, which was studied over the gold-functionalized monoliths. Here, gaseous streams of air and a H_2-CO-CO_2 mixture (of composition 74:1.4:24.6 % v/v, respectively) were dosed by using mass flow controllers. Alternatively, the feed to the reactor could be switched to a reducing / inert gaseous stream. After collecting the condensable components from the reactor (when present), the gaseous effluent stream was quantitatively evaluated in terms of volumetric total flowrate (bubble soap meter) and composition. A gas chromatograph (HP 4890D) equipped with Porapak Q and Carbosieve S-II columns and a TCD detector was profited here to measure on-line gas concentrations.

3 Results and discussion

3.1 Preparation of monolithic catalysts

The aluminum monolith prepared according to the method described in Section 2.1. presented a specific surface area of 40.7 m^2/g and a pore radius of 18.7 Å. The thickness of the alumina layer was 17 µm, with a generated oxide mass of 36.3 g/m^2. Figure 1 shows the SEM image of the metal substrate. The surface was uniform and presented whiskers of about 100 nm, providing a high degree of roughness to the metallic surface. This substrate has the characteristics to

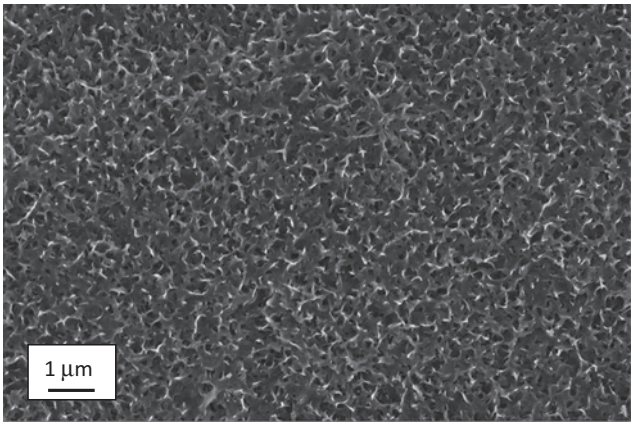

Figure 1: SEM image of the metal substrate after hydrothermal treatment.

achieve a good anchoring of the catalytic coating, and it also has a large surface area for incorporating the active phase by impregnation.

TiO_2 and Cu-Zn were deposited on the monolithic substrate. The catalyst loading, the results of the adherence test (for the cases of interest) and the surface area of the samples are presented in Table 1.

Table 1: Characteristics of the monolithic catalysts.

Monolith	Catalyst loading (mg)*	Adherence (%)	BET surface area (m^2 $g^{-1}_{monolith}$)
TiO_2-HS	4.5	–	–
TiO_2-IWI	50.0	97	44.6
Cu-Zn-HS	33.0	–	–
Cu-Zn-IWI	53.2	100	9.2

Note: * After calcination.

Table 1 shows that IWI synthesis allowed for the deposition of a larger amount of catalytic material than HS for both TiO_2 and Cu-Zn (under the synthesis conditions adopted in this work). IWI-synthesized monoliths were subjected to an adherence test as the mechanical stability of the catalyst coatings in monoliths is a decisive subject. They showed a very high adherence of the catalyst coatings to the surface of the substrate. After 30 min of ultrasound exposure, no weight loss was detected for Cu-Zn-IWI, and only approximately 3 % for TiO_2-IWI. The BET surface area of TiO_2-IWI and Cu-Zn-IWI were 44.6 and 9.2 m^2g^{-1}, respectively.

The dispersion and homogeneity of the catalytic deposits were studied by scanning electron microscopy (SEM). Figure 2 shows SEM images corresponding to the surface of TiO_2–IWI, Cu-Zn-IWI, TiO_2–HS and Cu-Zn-HS monoliths (Figure 2(a) to 2(d), respectively). TiO_2-IWI structured catalyst presented a homogeneous catalytic coating, with presence of agglomerated particles (Figure 2(a)). TiO_2-HS is similar in morphology to the support, consequently with the low catalyst loading (Figure 2(c) and Table 1). On the other hand, Cu-Zn-IWI exhibited good dispersion of the deposited particles with a homogeneous surface coating (Figure 2(b)) in comparison with Cu-Zn-HS (Figure 2(d)).

Energy dispersive X-ray analysis (EDX) was performed in order to analyze the surface composition of the catalytic layer. Based on the results for TiO_2-IWI presented in Figures 3(a) and 3(b), it could be determined that TiO_2 was present in the homogeneous coating and in the agglomerated particles (marked areas in the pictures). Figure 3(c) shows the presence of Cu and Zn. Ledesma and Llorca (2009) reported that the occurrence of Cu is always associated with the presence of Zn, indicating that an intimate contact exists between the two metals.

The metallic loading of the Au/TiO_2-IWI catalyst was 2 wt% (with respect to oxide support). Figure 4 shows a representative HRTEM image of gold nanoparticles on TiO_2-IWI. Round-shaped particles of about 5 nm are well dispersed over the TiO_2 support. Lattice fringes at 2.36 and 3.52 Å correspond to fcc (111) and (101) planes of Au and titania support, respectively.

3.2 Catalytic test: methanol steam reforming

The prepared Cu-Zn-IWI monolithic catalysts were studied towards H_2-rich gas production by methanol steam reforming (MSR). Due to simplicity reasons in the reactor set-up, diluted feeds were investigated in a first step. Before reaction, samples were reduced with 10 % H_2 in N_2 at 300 °C for 2 h (heating rate 8 °C/min).

Figure 5 reports the catalytic performance as influenced by the residence time (W/F_T). As mentioned above, a N_2-diluted methanol + water feed (2 % v/v) was adopted, with a steam-to-carbon ratio (S/C) equal to 1.5. Figure 5(a) shows values of methanol conversion (X_{MeOH}) and hydrogen yield (η_{H2}), whereas Figure 5(b) presents carbon oxides selectivities as calculated by the following equation:

$$S_{co_x} = \frac{F_{co_x}}{F_{co_2} + F_{co}} 100 \qquad where\ x = 1, 2 \qquad (1)$$

As seen in Figure 5(a), as the feed load (F_T) is decreased (i. e., increasing the residence time), methanol conversion

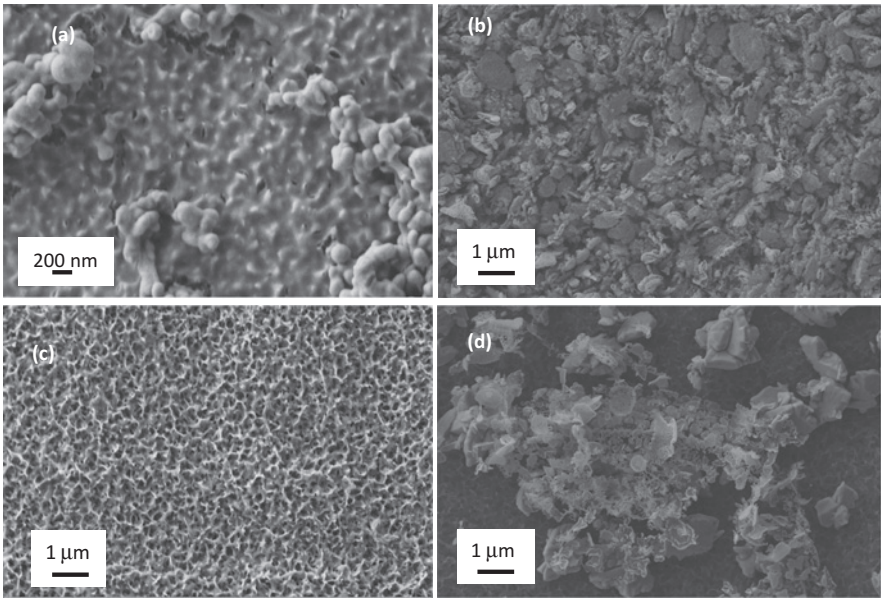

Figure 2: SEM images of (a) TiO_2-IWI, (b) Cu-Zn-IWI, (c) TiO_2-HS, and (d) Cu-Zn-HS.

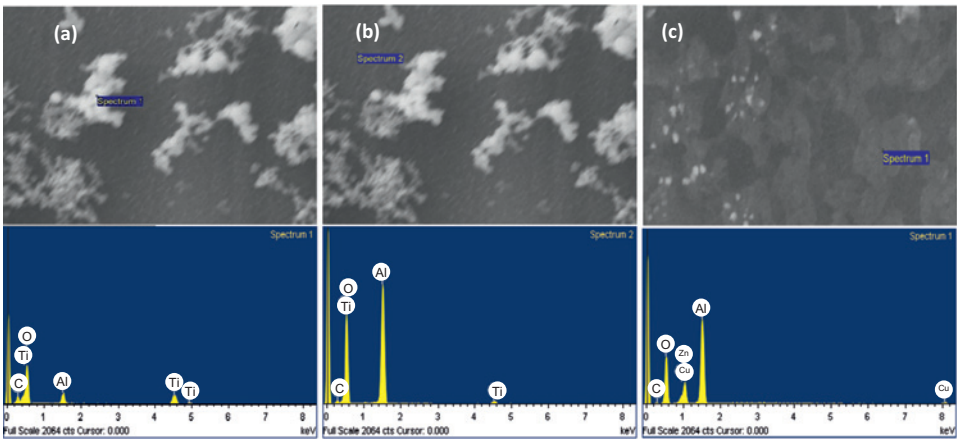

Figure 3: SEM images (above) and EDX results (below) for the selected area. References: (a) and (b) TiO_2-IWI, (c) Cu-Zn-IWI.

is favored, reaching high to very high values for the operating conditions selected. Moreover, the hydrogen yield does not present an analogous monotonically increasing trend with the residence time. In fact, the η_{H2} shows a maximum over the residence time ($5{\cdot}10^{-3}$ $kg_{cat}.s.mmol^{-1}$), increasing from lower W/F_T, leading to higher methanol conversion and hence higher amounts of H_2 are generated per unit methanol in feed. On the other hand, lower enough loads permit almost complete methanol conversions and the reverse water-gas shift (R-WGS) reaction acts towards the shift equilibrium due to the high amounts of hydrogen present and generating increasing amounts of CO at the expense of CO_2, as seen in Figure 5(b).

The effect of operating temperature on the methanol conversion and hydrogen yield is reported in Figure 6. Diluted feeds are selected here as well, with a residence time of $W/F_T = 5{\cdot}10^{-3}$ $kg_{cat}.s.mmol^{-1}$ (where the maximum of Figure 5 was observed). Temperature affects positively methanol conversion not only based on kinetics but also in equilibrium displacement as methanol steam reforming is an endothermic equilibrium-limited reaction. Conversely, and resembling the argumentation given to explain the results shown in Figure 5(a) and 5(b), a maximum in η_{H2} is once more observed. At low temperature, higher methanol conversion leads to higher H_2 yield. As the temperature increases from ca. 570 K, the H_2 yield reaches a plateau

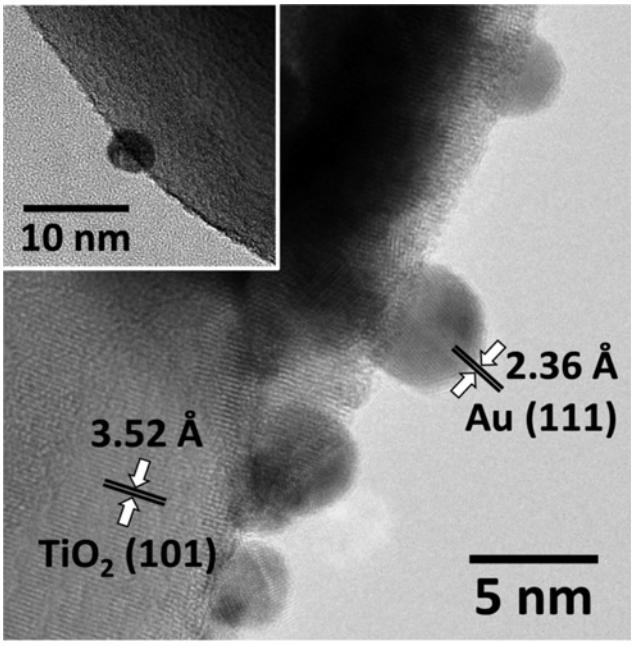

Figure 4: HRTEM images of gold nanoparticles on TiO_2-IWI.

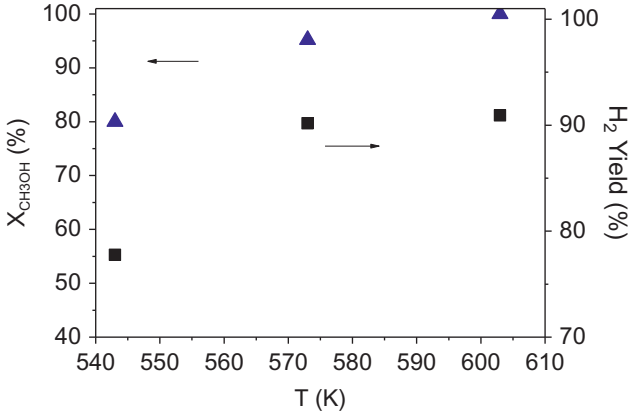

Figure 6: Influence of the temperature on methanol conversion (▲) and hydrogen yield (■). $W/F_T = 5{\cdot}10^{-3}$ $kg_{cat}.s.mmol^{-1}$ and $H_2O/CH_3OH = 1.5$.

(and most probably diminishes for higher temperatures than those investigated in this paper) due to the preponderance of the R-WGS reaction.

In order to explore the catalytic performance of the Cu-Zn-IWI monoliths under more realistic conditions, experimental set-up Scheme 2 was used, implying non-diluted feeds. Figure 7 shows results concerning MSR for the mentioned feed conditions and two different operating temperatures. Methanol conversion to carbon oxides (i. e., CO and CO_2) and hydrogen yield are presented in Figure 7(a) and 7(b), respectively. For comparison purposes, results corresponding to diluted feed (experimental set-up Scheme 1) are included as well. As already discussed, higher temperatures lead to an increase in methanol conversion to CO/CO_2 for both feed systems (see Figure 7(a)). However, the conversion levels for the case when non-diluted feed is selected are lower than the ones for diluted feed. In the former case, the amount of methanol to be processed is higher. Additionally, MSR is an equilibrium-limited reaction with increasing number of moles which determines that equilibrium is shifted to higher conversions as dilution increases (i. e., as the molar fraction of the inert in-feed increases). Although the mentioned drop in conversion is noticeable, the achieved conversion levels are comparable with values reported in the literature. Du et al. (2012) report a methanol conversion of ca. 60 % for a feed rate of $6.5{\cdot}10^{-2}$ l/h and S/C = 1.3. In other work, Iulianelli et al. (2014) report methanol conversions higher than 50 % for concentrated feed and temperatures ranged between 573 K and 603 K. Figure 7(b) shows the hydrogen yield increase with

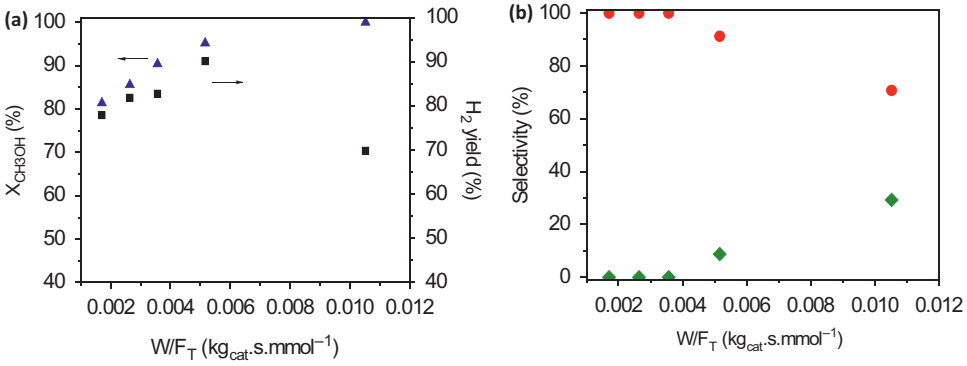

Figure 5: Influence of W/F_T on (a) methanol conversion (▲) and hydrogen yield (■), (b) CO (◆) and CO_2 (●) selectivity. T = 573 K and $H_2O/CH_3OH = 1.5$.

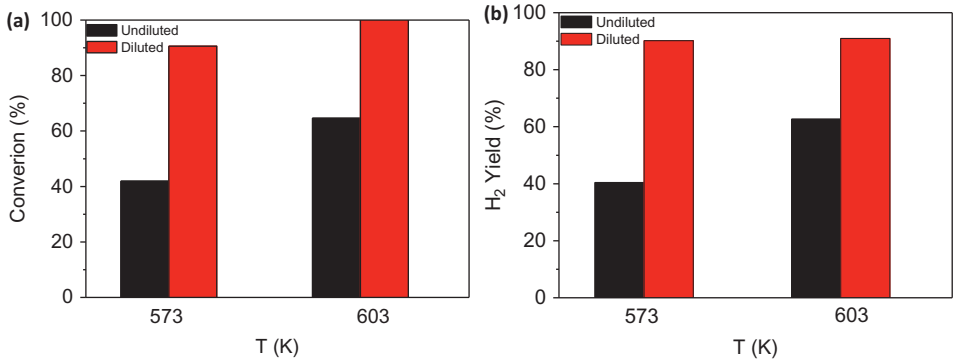

Figure 7: Influence of temperature for diluted and non-diluted feed mixture on (a) methanol conversion (b) and hydrogen yield. $W/F_T = 5{\cdot}10^{-3}\,kg_{cat}.s.\,mmol^{-1}$ and $H_2O/CH_3OH = 1.5$.

temperature for undiluted feed as conversion levels are far from complete. The constancy in η_{H2} for diluted feeds was already explained above in terms of the enhancement of the R-WGS reaction.

Finally, a study including the comparison of feed operating schemes as influenced by the residence time was accomplished. Once again, Figure 8(a) presents methanol conversion while H_2 yield is reported in Figure 8(b). Higher residence times promote higher conversions for both systems. Interestingly, an opposite trend in terms of H_2 yield was measured under the selected operating conditions for both feeds. As a diluted feed is not favored here at high residence time due to the influence of the R-WGS reaction for which H_2 is a reactant, operation with concentrate feed is positively affected by the residence time as methanol conversion is not complete for both residence times studied. A H_2 yield slightly lower than 60 % at $W/F_T = 1{\cdot}10^{-2}\,kg_{cat}.s.\,mmol^{-1}$ deserves to be remarked for a non-diluted feed operation (although methanol conversion to CO_x amounts here 55 %).

XPS study was performed in order to investigate the oxidation states of Cu and Zn, and the elemental surface composition of the catalyst before and after reaction. Table 2 compiles binding energy values and surface elemental ratios obtained over the samples.

Table 2: Binding energies (BE), Kinetic energy (KE) and surface atomic ratios determined by XPS over Cu-Zn-IWI catalyst.

Sample	BE Cu $2p_{3/2}$ (eV)	BE Zn $2p_{3/2}$ (eV)	KE Zn LMM (eV)	Cu/Zn
Fresh	931.8	1,021.9	988.3	0.11
Spent	932.9	1,021.1	988.7	0.28

For the fresh sample, it can be noted (Figure 9) a signal at 931.8 eV associated with the BE of Cu $2p_{3/2}$ and the thorough absence of the satellite peak of the Cu $2p_{3/2}$ band. The latter indicates the existence of metallic copper (Chinchen, Waugh, and Whan 1986). Figure 10 shows the X-ray

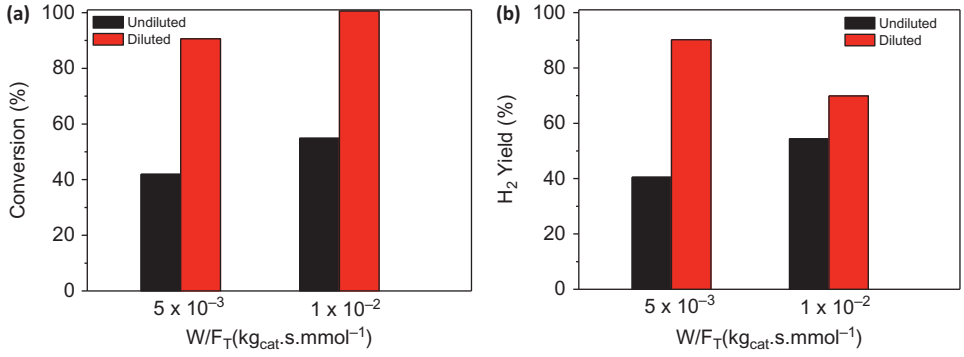

Figure 8: Influence of residence time for diluted and non-diluted feed mixture on on (a) methanol conversion (b) and hydrogen yield. Operating conditions: T = 573 K and $H_2O/CH_3OH = 1.5$.

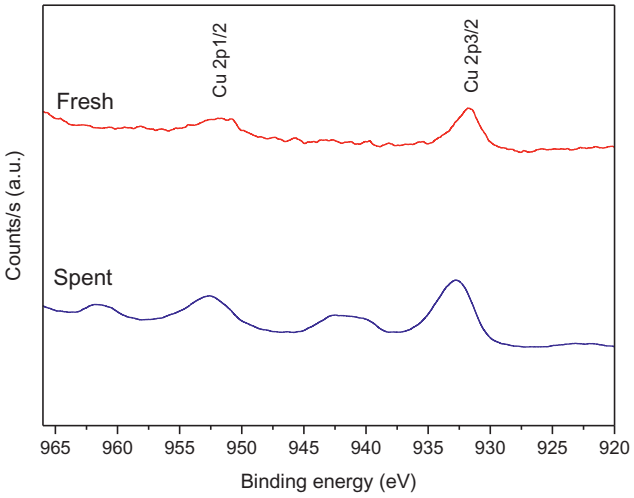

Figure 9: X-ray photoelectron spectra of the Cu $2p_{3/2}$ region of fresh and spent catalysts.

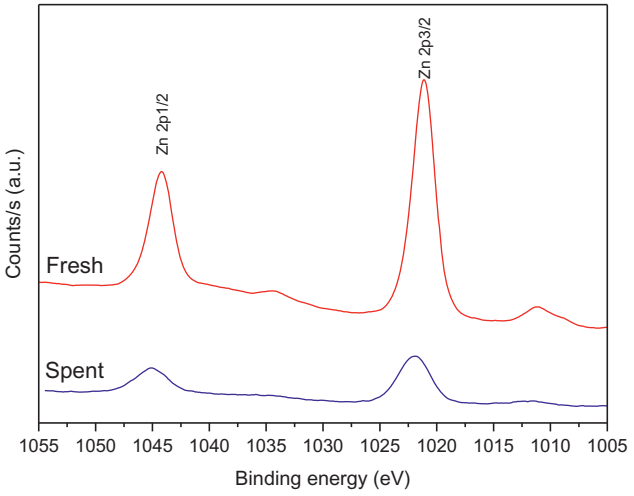

Figure 10: X-ray photoelectron spectra of the Zn $2p_{3/2}$ region of fresh and spent catalysts.

photoelectron spectra of the Zn $2p_{3/2}$ region of fresh and spent catalysts. The distinction between the Zn(0) and Zn(II) species using the photoemission Zn $2p_{3/2}$ is not simple, since they display similar binding energies: 1,021.8–1,022.0 eV for metallic Zn and 1,021.8–1,022.5 eV for ZnO (Lenarda et al. 2006). The chemical state of Zn can be identified using the Zn LMM Auger signal and determining the modified Auger parameter (α). This parameter was calculated using the following equation:

$$a = EK\ Zn\ LMM + EB\ Zn2p_{3/2} \quad (2)$$

where KE Zn LMM is the kinetic energy of the Auger electron of Zn LMM. The calculated α value was 2,010.2 eV, indicating the presence of ZnO (Briggs and Seah 1990).

For the spent catalyst, the Cu $2p_{3/2}$ signal at 932.9 eV shows in Figure 9 the shakeup satellite (located about 10 eV higher than the Cu $2p_{3/2}$ transition) indicating the presence of Cu^{2+} (Kim 1974), formed under the steam reforming atmosphere. Cu oxidation in the reaction medium could be attributed to the presence of steam at high temperatures or copper reoxidation when the reaction finished. For zinc, the modified Auger parameter was 2,009.8 eV denoting the existence of ZnO (Briggs and Seah 1990), as expected.

The values of the surface composition were estimated from the Cu $2p_{3/2}$ and Zn $2p_{3/2}$ signals, using the appropriate sensitivity correction factors. As shown in Table 2, the surface Cu/Zn atomic ratio was different to the bulk ratio for both samples. The Cu surface composition was lower than the bulk. This indicates a high Zn segregation (Daia et al. 2001).

To summarize, methanol steam reforming was studied over the developed metallic monoliths functionalized with Cu-Zn by the IWI deposition method. The samples showed promissory results in terms of activity and selectivity, operating for more than 28 h without signs of deactivation. Both diluted and concentrated methanol + water feeds were assayed. Complete methanol conversion was achieved for diluted feed. Maximum methanol conversions of 55 % with 60 % H_2 yield were measured when concentrated feed was selected. XPS characterization did not show noticeable differences between spent and fresh catalyst.

3.3 Catalytic test: CO-PrOx

As previously stated, gold nanoparticles were reported as highly active and with appropriate selectivity to conduct the preferential oxidation of CO in H_2-rich environments at low operating temperatures (when compared with conventional Pt-based PrOx catalysts). However, it was also reported that Au-based catalysts suffer from deactivation, mainly due to sintering of the Au nanoparticles. In order to test the stability of the proposed Au/TiO_2-IWI structure sample, the catalytic performance was measured for the same operating conditions at three different times during the experimentation after reducing the sample under 10 % H_2 in N_2 at 300 °C for 2 h (heating rate 8 °C/min). Figure 11 shows the results from these experiences. As seen, both stable levels of CO conversion and selectivity to CO_2 (see eq. (3)) were maintained for at least 30 h operation (which covers all the tests studied in this contribution).

The effect of the operating temperature over conversion and selectivity is presented in Figure 12. As shown,

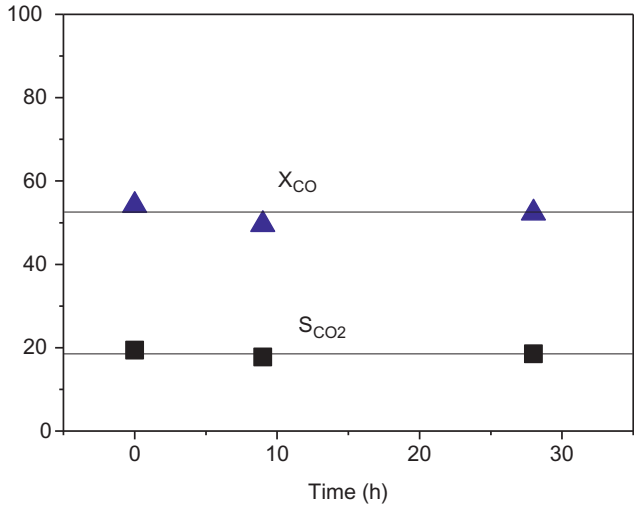

Figure 11: CO-PrOx stability test. Operating conditions: T = 363 K, W = 100 mg, F_T = 40 ml.min^{-1}.

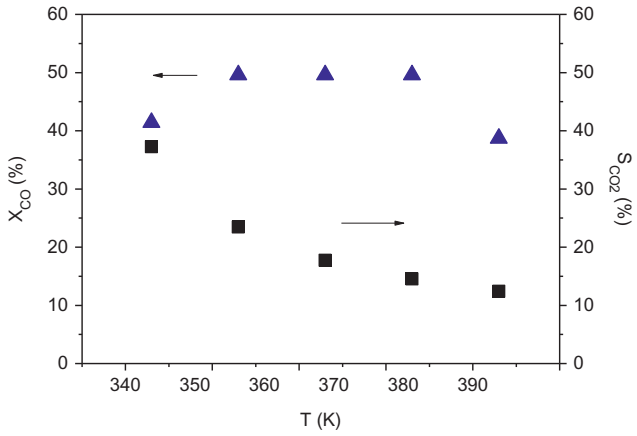

Figure 12: Temperature effect over CO conversion (X_{CO}) and CO_2 selectivity (S_{CO2}). Operating conditions: λ = 3, F_T = 40 ml.min^{-1}.

CO conversion does not present a monotonous behavior with the temperature. In fact, temperature increases from low values lead to an increase in conversion based on kinetic reasons. On the other hand, as temperature increases (T ≥ 373 K in this case) the selectivity deteriorates and the O_2 is increasingly consumed by the non-desired H_2 oxidation, rendering enhanced amounts of unconverted CO. This behavior obeys to the fact that the activation energy of H_2 oxidation is higher than that of the CO oxidation, as reported elsewhere for CO-PrOx over gold-based catalysts (Lindström and Pettersson 2002).

The parameter λ, as defined by eq. (4), is commonly used in CO-PrOx to quantify the oxygen excess in feed, where λ = 1 is the stoichiometric relation to only oxidize the CO fed.

$$S_{co_2} = \frac{(F_{co}^{in} - F_{co})}{2(F_{o_2}^{in} - F_{o_2})} \quad (3)$$

$$\lambda = \frac{2F_{o2}^{in}}{F_{co}^{in}} \quad (4)$$

Figure 13 reports results of the influence of λ in the catalytic performance. As λ is increased, more O_2 is available to oxidize the CO and, consequently, CO conversion increases. However, the selectivity to CO_2 drops as λ shifts from 3 to 5.1. As reported by Mariño, Descorme, and Dupez (2004), a high O_2 excess enhances H_2 oxidation rate. It should be noted that this effect is not observed when λ is changed from 1.1 to 3 as in the first case O_2 was depleted within the reactor.

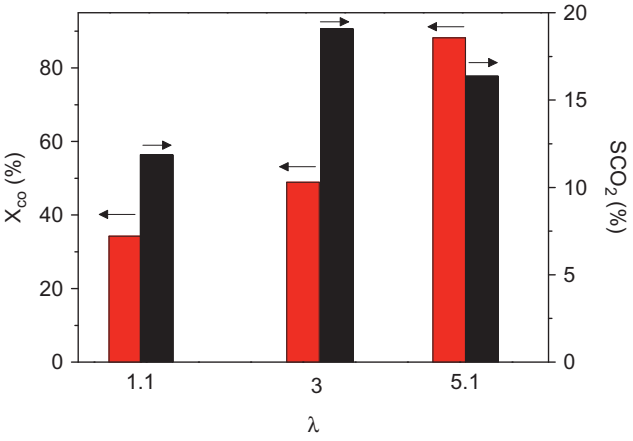

Figure 13: Influence of λ over CO conversion (X_{CO}) and CO_2 selectivity (S_{CO2}). T = 363 K.

It is worth remarking that the influence of the reverse or direct water-gas shift reaction should be neglected here due to the low operation temperatures at hand.

Overall, promissory results were also achieved for the gold-based catalyst in the CO preferential oxidation in a H_2-rich atmosphere. Although CO conversions of ca. 60 % were achieved here, operation with higher catalyst loadings would be recommendable (i. e., larger volumes of monoliths) to reach the high CO conversions required for PrOx catalysts.

X-ray photoelectron spectroscopy was used to investigate the oxidation states of Au and the elemental surface composition following synthesis and reduction, and after reaction test. Both for the fresh and spent samples, two sharp peaks at 86.5 and 83.0 eV were recorded (Figure 14), which are characteristic of spin–orbit splitting (Au $4f_{5/2}$ and $4f_{7/2}$, respectively) of Au core level spectra consistent with the Au^0 oxidation state (Chou, McFarland 2004). The Au $4f_{7/2}$ binding energy obtained

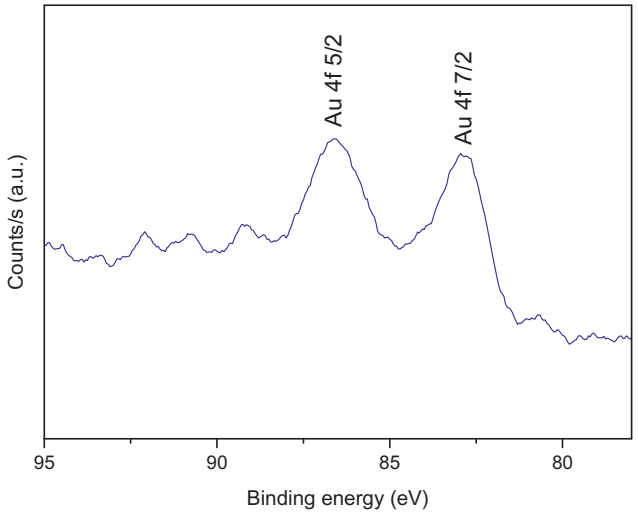

Figure 14: X-ray photoelectron spectra of the Au 4f region of spent catalysts.

is slightly lower than the reported values. It has to be considered that the observed signal is small and broad, which could be consequence of the presence of disperse Au nanoparticles (Louis 2008). The Au/Ti surface atomic ratio was 0.004 for the fresh samples, and no significant difference was detected after reaction test. This values is in agreement with previous works (Murdoch et al. 2011).

4 Conclusions

Catalytic monoliths containing Cu-Zn and Au/TiO_2 supported on anodized aluminum monoliths (AAMs) were prepared, characterized by SEM, EDX, HRTEM and XPS tested for mechanical stability, and studied in two different test reactions, namely, methanol steam reforming (MSR) and preferential oxidation of carbon monoxide (CO-PrOx).

It was possible to generate a surface with whiskers and enhanced surface area by a hydrothermal treatment of the AAMs. IWI synthesis allowed for a larger deposition of catalytic material than HS, with very good adhesion. The TiO_2-IWI structured catalyst presented a homogeneous catalytic coating, with the presence of agglomerated particles. On the other hand, Cu-Zn-IWI showed good dispersion of the deposited particles with a homogeneous surface coating.

MSR was studied over the developed metallic monoliths functionalized with Cu-Zn by the IWI deposition method. The samples showed promising results in terms of activity, selectivity, and stability. Both diluted and concentrated methanol + water feeds were assayed. Complete methanol conversion was achieved for the diluted feed. Maximum methanol conversions of 55% with 60% H_2 yield were measured when the concentrated feed was selected. Promising results were also achieved for the Au-based structured catalysts for the CO-PrOx in an H_2-rich atmosphere. Although CO conversions of approximately 60% were achieved, operation with higher catalyst loadings would be recommended to reach the high CO conversions required for PrOx catalysts.

Funding: The authors want to thank the financial support from Consejo Nacional de Investigaciones Científicas y Técnicas (CONICET) and Ministerio de Ciencia, Tecnología e Innovación Productiva (MINCyT) from Argentina (MINCYT-MICINN 2011: ES/11/07), and MINECO project ENE2015-63969-R (Spain). Thanks are given to ANPCyT for the purchase of the SPECS multitechnique analysis instrument (PME8-2003). J.L. is Serra Húnter Fellow and is grateful to ICREA Academia program.

References

1. Agrell, J., Birgersson, H., Boutonnet, M., 2002. Steam reforming of methanol over a Cu/ZnO/ Al_2O_3 catalyst: a kinetic analysis and strategies for suppression of CO formation. Journal of Power Sources 106, 249–257.
2. Bamwenda, G.R., Tsubota, S., Nakamura, T., Haruta, M., 1997. The Influence of the Preparation Methods on the Catalytic Activity of Platinum and Gold Supported on TiO_2 for CO Oxidation. Catalysis Letters 44, 83–87.
3. Bichon, P., Asheim, M., Jordal, A., Sperle, T., Fathi, M., Holmen, A., Blekkan, E.A., 2007. Hydrogen from methanol steam-reforming over Cu-based catalysts with and without Pd promotion. International Journal of Hydrogen Energy 32 (12) 1799–1805.
4. Briggs, D., Seah, M.P. (Eds.). 1990. Practical Surface Analysis, 2nd ed., vol I, auger and X-ray photoelectron spectroscopy. John Wiley, New York.
5. Chinchen, G.C., Waugh, K.C., Whan, D.A., 1986. The activity and state of the copper surface in methanol synthesis catalyst. Applied Catalyst 25, 101–107.
6. Chou, J., McFarland, E.W., 2004. Direct propylene epoxidation on chemically reduced Au nanoparticles supported on titania. Chemical Communications 14, 1648–1649.
7. Cybulski, A., Moulijn, J.A., 1998. Structured Catalysts and Reactors, Marcel Dekker, New York.
8. Daia, W.L., Suna, Q., Denga, J.F., Wub, D., Sunb, Y.H., 2001. XPS studies of Cu/ZnO/Al_2O_3 ultra-fine catalysts derived by a novel gel oxalate co-precipitation for methanol synthesis by $CO_2 + H_2$. Applied Surface Science 177, 172–179.
9. Daté M., Haruta M., 2001. Moisture Effect on CO Oxidation over Au/TiO_2 Catalyst. Journal of Catalysis 201, 221–224.
10. Divins, N.J., López, E., Roig, M., Trifonov, T., Rodríguez, A., González de Rivera, F., Rodríguez, L.I., Seco, M., Rossell, O., Llorca, J., 2011. A million-channel CO-PrOx microreactor on a fingertip for fuel cell application. Chemical Engineering Journal 167, 597–602.

11. Du, X., Shen, Y., Yang, L., Shi, Y., Yang, Y., 2012. Experiments on hydrogen production from methanol steam reforming in the microchannel reactor. International Journal of Hydrogen Energy 37, 12271 –12280.
12. Galletti, C., Fiorot, S., Specchia, S., Saracco G., Specchia V., 2007. Catalytic performance of Au/TiO_2 catalyts prepared by deposition-precipitation for CO preferential oxidation in H_2-rich gases. Chemical engineering Journal 134, 45–50.
13. Iulianelli, A., Ribeirinha, P., Mendes, A., Basile, A., 2014. Methanol steam reforming for hydrogen generation via conventional and membrane reactors: a review. Renewable and Sustainable Energy Reviews 29, 355–368.
14. Kim, K.S., 1974. Charge transfer transition accompanying X-ray photoionization in transition-metal compounds. Journal of Electron Spectroscopy and Related Phenomena 3, 217–226.
15. Kipnis, M., 2014. Gold in CO oxidation and PROX: the role of reaction exothermicity and nanometer-scale particle size. Applied Catalysis B: Environmental 152–153, 38–45.
16. Lakshmanan, P., Park, J.E., Park, E.D., 2014. Recent advances in preferential oxidation of CO in H_2 over gold. Catalysis Surveys from Asia, 18(2), 75–88.
17. Ledesma, C., Llorca, J., 2009. Hydrogen production by steam reforming of dimethyl ether over Cu–Zn/CeO_2–ZrO_2 catalytic monoliths. Chemical Engineering Journal 154, 281–286.
18. Lenarda, M., Moretti, E., Storaro, L., Patrono, P., Pinzari, F., Rodríguez-Castellón, E., Jiménez-López, A., Busca, G., Finocchio, E., Montanari, T., Frattini, R., 2006. Finely dispersed Pd-Zn catalyst supported on an organized mesoporous alumina for hydrogen production by methanol steam reforming. Applied Catalysis A: General 312, 220–228.
19. Lindström, B., Pettersson, L.K., 2002. Steam reforming of methanol over copper-based monoliths: the effects of zirconia doping. Journal of Power Sources 106(1–2) 264–273.
20. Lopez, L., Kolios, G., Eigenberger, G., 2005. Structured folded-plate reactor for CO preferential oxidation. Industrial & Engineering Chemistry Research 44, 9659–9667.
21. Lopez, L., Kolios, G., Eigenberger, G., 2007. Preferential oxidation in a folded-plate reactor. Chemical Engineering Science 44, 9659–9667.
22. Louis, C., 2008. Gold nanoparticles: recent advances in CO oxidation, in: Astruc, D. (Ed.), Nanoparticles and Catalysis. WILEY-VCH Verlag GmbH & Co. KGaA, Weinheim, pp. 483.
23. Mariño, F., Descorme, C., Dupez, D., 2004. Noble metal catalysts for the preferential oxidation of carbon monoxide in the presence of hydrogen (PROX). Applied Catalysis B: Environmental 54, 59–66.
24. Murdoch, M., Waterhouse, I.N., Nadeem, M.A., Metson, J.B., Keane, M.A., Howe, R.F., Llorca, J., Idriss, H., 2011. The effect of gold loading and particle size on photocatalytic hydrogen production from ethanol over Au/TiO_2 nanoparticles. Nature Chemistry 3, 489–492.
25. Purnama, H., Ressler, T., Jentoft, R.E., Soerijanto, H., Schlögl, R., Schomäcker, R., 2004. CO formation/selectivity for steam reforming of methanol with a commercial CuO/ZnO/Al. Applied Catalysis A: General 259, 83–94.
26. Reddy, E., Lee, H., Kim, D., 2015. Steam reforming of methanol over structured catalysts prepared by electroless deposition of Cu and Zn on anodically oxidized alumina. International Journal of Hydrogen Energy 40, 2509–2517.
27. Sá, S., Silva H., Brandao L., Sousa J., Mendes A., 2010. Catalysts for metanol steam reforming-a review. Applied Catalysis B: Enviromental 99, 43–57.
28. Sanz, O., Almeida, L., Zamaro, J., Ulla, M., Miró, E., Montes, M. 2008. Washcoating of Pt-ZSM5 onto aluminium foams. Applied Catalysis B: Environmental 78, 166–175.
29. Schumacher, B., Denkwitz, Y., Plzak, V., Kinne, M., Behm, R.J., 2004. Kinetics, mechanism, and the influence of H_2 on the CO oxidation reaction on a Au/TiO_2 catalyst. Journal of Catalysis 224, 449–462.
30. Tsubota, S., Cunningham, D., Bando, Y., Haruta, M., 1993. CO oxidation over gold supported on TiO_2, in: T. Inui et al. (Eds.), New Aspects of Spillover Effect in Catalysis. The Netherlands: Elsevier Science Publishers B.V. 325–328.
31. Turco, M., Bagnasco, G., Cammarano, C., Senese, P., Costantino, U., Sisani, M., 2007. Cu/ZnO/Al_2O_3 catalysts for oxidative steam reforming of methanol: The role of cu and the dispersing oxide matrix. Applied Catalysis B: Environmental 77, 46–57.
32. Wu, G.-S., Mao, D.-S., Lu, G.-Z., Cao, Y., Fan, K.-N., 2009. The role of the promoters in Cu based catalysts for methanol steam reforming. Catalysis Letters 130, 177–184.